Article
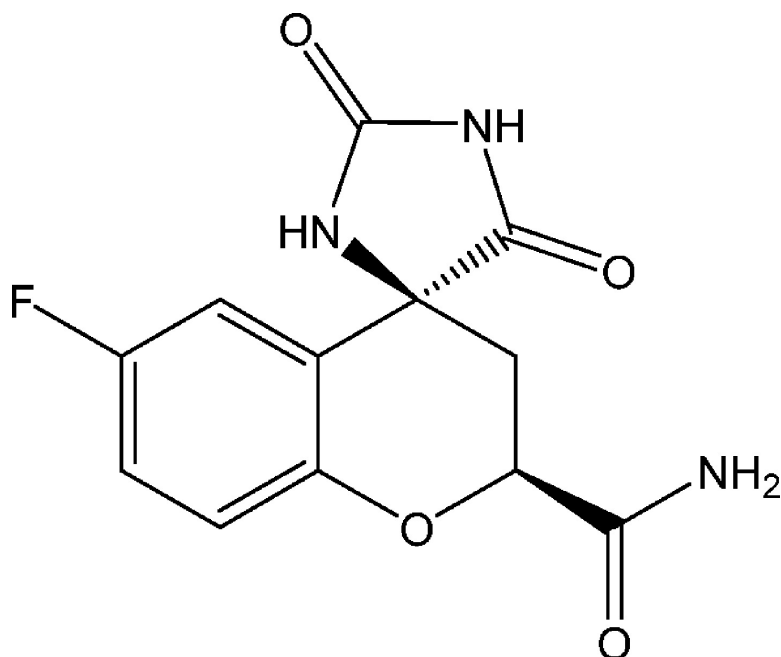
Structure of Aldehyde Reductase Holoenzyme in Complex with the Potent Aldose Reductase Inhibitor Fidarestat: Implications for Inhibitor Binding and Selectivity

Ossama El-Kabbani, Vincenzo Carbone, Connie Darmanin, Mitsuru Oka, Andre Mitschler, Alberto Podjarny, Clemens Schulze-Briese, and Roland P.-T. Chung

More About This Article

Additional resources and features associated with this article are available within the HTML version:

- Supporting Information
- Links to the 3 articles that cite this article, as of the time of this article download
- Access to high resolution figures
- Links to articles and content related to this article
- Copyright permission to reproduce figures and/or text from this article

Journal of
Medicinal Chemistry

View the Full Text HTML

ACS Publications
High quality. High impact.

Structure of Aldehyde Reductase Holoenzyme in Complex with the Potent Aldose Reductase Inhibitor Fidarestat: Implications for Inhibitor Binding and Selectivity

Ossama El-Kabbani,*,† Vincenzo Carbone,† Connie Darmanin,† Mitsuru Oka,# Andre Mitschler,§ Alberto Podjarny,§ Clemens Schulze-Briese,‡ and Roland P.-T. Chung†

Department of Medicinal Chemistry, Victorian College of Pharmacy, Monash University (Parkville Campus), 381 Royal Parade, Vic 3052, Australia, Sanwa Kagaku Kenkyusyo Company, Ltd., 363, Shiosaki, Hokusei-cho, Inabe-shi, Mie 511-0406, Japan, Departement de Biologie et Genomique Structurale, IGBMC, CNRS INSERM ULP, 1 Rue Laurent Fries, B.P. 163, 67404 Illkirch, France, and Swiss Light Source at PSI, 5232 Villigen, Switzerland

Structure determination of porcine aldehyde reductase holoenzyme in complex with the potent aldose reductase inhibitor fidarestat was carried out to explain the difference in the potency of the inhibitor for aldose and aldehyde reductases. The hydrogen bonds between the active-site residues Tyr50, His113, and Trp114 and fidarestat are conserved in the two enzymes. In aldose reductase, Leu300 forms a hydrogen bond through its main-chain nitrogen atom with the exocyclic amide group of the inhibitor, which when replaced with a Pro in aldehyde reductase, cannot form a hydrogen bond, thus causing a loss in binding energy. Furthermore, in aldehyde reductase, the side chain of Trp220 occupies a disordered split conformation that is not observed in aldose reductase. Molecular modeling and inhibitory activity measurements suggest that the difference in the interaction between the side chain of Trp220 and fidarestat may contribute to the difference in the binding of the inhibitor to the enzymes.

Introduction

Aldehyde reductase (ALR1, EC 1.1.1.2) belongs to the aldo−keto reductase (AKR) superfamily of enzymes whose members are responsible for a wide variety of biological functions. These include the regulation of the proinflammatory response via the reduction of aldehyde phospholipids,[1] the synthesis of metabolically vital compounds such as prostaglandins,[2,3] and the modulation and modification of steroids in vivo,[4−7] which include progesterone signaling in breast mammary cells.[8] Members of the AKR superfamily are composed of approximately 315−330 residues and generally form monomeric proteins with a molecular weight of 36 kDa.[9,10] While ALR1 prefers the reduction of aromatic rather than aliphatic aldehydes,[11] both ALR1 and the homologous aldose reductase (ALR2, EC 1.1.1.21) catalyze the NADPH-dependent reduction of aldehydes, xenobiotic aldehydes, ketones, trioses, and triose phosphates.[9,10,12−15] The two enzymes have been isolated and purified from a number of tissues including the brain, kidney, liver, lens, and skeletal muscle.[16−18] Moreover, ALR1 and ALR2 share a high degree of sequence (∼65%) and structural homology[19] with the majority of the differences present at the C-terminal end of an α/β-TIM barrel structure,[20] which is the region responsible for substrate and inhibitor specificity in the AKRs.[21] Earlier studies indicated that most known ALR2 inhibitors (ARIs) inhibit ALR1 and illustrated

that the active sites of both enzymes contain common characteristics in the manner by which they bind substrate and inhibitor.[19,22]

ALR2 has been identified as the first enzyme involved in the polyol pathway of glucose metabolism that converts glucose into sorbitol, the rate-limiting step of the pathway.[23] Glucose overutilization through the polyol pathway has been linked to tissue-based pathologies associated with diabetes complications,[24,25] including cataract formation,[26] peripheral neuropathy,[27] and diabetes-linked kidney lesions.[28] These chronic pathologies make the development of a potent ARI an obvious and attractive strategy to prevent or delay the onset and progression of the complications. To date, none of the currently available ARIs have been approved for clinical use (outside of Japan) because of toxicity problems and lack of specificity toward the target enzyme.[29] An ARI specificity is often determined by measuring its activity against ALR1, an enzyme that metabolizes 3-deoxyglucosone and methylglyoxal, which are intermediates for the formation of the advanced glycation end products (AGEs).[30,31] Thus, ALR1 inhibition may account for some of the undesirable side effects associated with the present ARIs.

Recent crystallographic and molecular modeling studies have shown that ARIs bind to the active sites of ALR1 and ALR2 with conserved hydrogen-bonding interactions between the polar heads of the inhibitors and the active-site residues Tyr50, His113, and Trp114.[22,32−38] The difference in inhibitor potency for the two enzymes has been attributed to nonconserved residues located in the C-terminal loop lining a hydrophobic region of the active site called the "specificity pocket". We have previously reported the structure of human aldose

---

* To whom correspondence should be addressed. Phone: 61-3-9903-9691. Fax: 61-3-9903-9582. E-mail: Ossama.El-Kabbani@vcp.monash.edu.au.
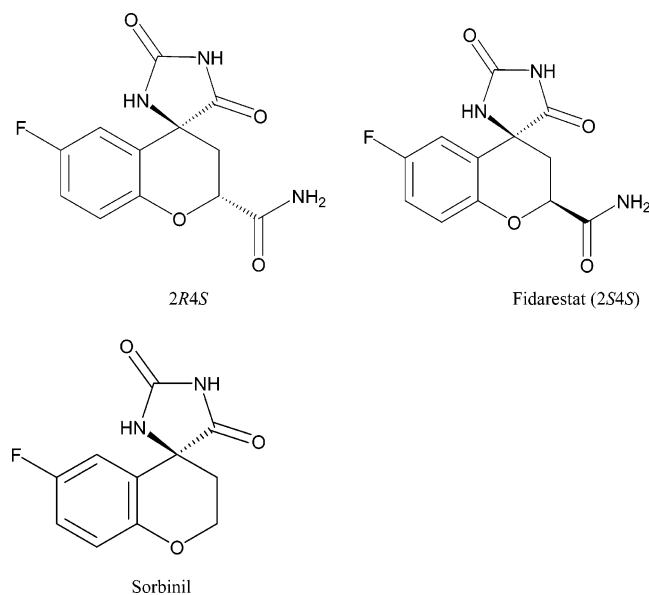† Monash University (Parkville Campus).
Sanwa Kagaku Kenkyusyo Company, Ltd.
§ IGBMC, CNRS INSERM ULP.
‡ Swiss Light Source at PSI.

Scheme 1

2R4S　　　　　　　　　　Fidarestat (2S4S)

Sorbinil

reductase holoenzyme in complex with the cyclic imide inhibitor fidarestat ((2S,4S)-6-fluoro-2′,5′-dioxospiro-[chroman-4,4′-imidazoline]-2-carboxamide) determined at an ultrahigh resolution of 0.92 Å, and proposed a mechanism for ALR2 inhibition based on the protonation states of the inhibitor and the catalytic residue His110.[36] In this study, we report the first high-resolution ternary structure of an aldehyde reductase in complex with fidarestat. The enzyme, isolated from porcine kidneys, shares 97% sequence homology and a conserved active-site structure with the human enzyme.[39] A comparison between the inhibitor-binding sites of ALR1 and ALR2, complemented with molecular modeling calculations and inhibitory activity measurements of fidarestat (2S4S), its 2R4S-isomer, and the ARI sorbinil, suggested that both Pro301 (Leu300 in ALR2) and the conserved Trp220, which occupies a double conformation in ALR1 but not in ALR2, account for the difference in the potency of the inhibitor for the two enzymes. This information may aid the structure-based design of ARIs that are more selective for ALR2 than ALR1 and have less toxicity problems than the currently available inhibitors. The chemical structures of fidarestat (2S,4S), its 2R,4S-isomer, and sorbinil are shown in Scheme 1.

Results and Discussion

X-ray Crystallography. The structure of porcine aldehyde reductase holoenzyme in complex with fidarestat was determined at 1.85 Å resolution, with final R_{cryst} and R_{free} values equal to 20.9% and 29.7%, respectively, similar to values reported for previous ALR1 structures.[40] Moreover, similar to previous X-ray structures,[39,40] the electron densities observed for both main chain atoms and side chain atoms in the segments containing residues 218−225 (loop B) and 304−308 (loop C) are weak compared to the rest of the molecule because of the flexibility of these regions. The asymmetric unit consisted of 324 amino acids, one NADPH coenzyme, one fidarestat molecule, 210 waters, and 1 sulfate molecule. A φ, ψ plot of main chain torsion angles placed approximately 96.7% and 3.3% of the

Table 1. Data Collection and Refinement Statistics

Data Collection and Processing	
no. of crystals used	1
wavelength (Å)	1.000
space group	$P6_522$
unit-cell parameters	
a, b, c (Å)	67.35, 67.35, 244.74
α, β, γ (deg)	90.0, 90.0, 120.0
resolution range (Å)	50−1.85
unique reflections	26 755
$R(I)_{merg}$ (overall) (%)	9.7
$R(I)_{merg}$ [a] (%)	31.4
completeness (overall) (%)	91.2
completeness[a] (%)	90.1
redundancy (overall)	3.3
redundancy[a]	3.7
$I/\sigma(I)$ (overall)	11.3
$I/\sigma(I)$[a]	3.8
Refinement	
resolution range (Å)	10−1.85
all reflections used	26 599
size R_{free} set (%)	5
all reflections (R_{free})	(1320)
R-values based on $F > 4\sigma_F$	
R_{cryst}/R_{free} (%)	20.9/29.7
protein residues	324
coenzyme	1
inhibitor	1
sulfate	1
water molecules	210
Root-Mean-Squared Deviations	
bonds (Å)	0.006
angles (deg)	1.799
dihedrals (deg)	14.460
Ramachandran Plot	
residues in most favored regions (%)	96.7
residues in additional allowed regions (%)	3.3
Estimated Coordinate Error	
Luzzati mean error (Å)	0.165
Mean B Factor (Å²)	
protein	21.1
coenzyme	12.9
inhibitor	20.5
sulfate	37.3

[a] Data in the highest resolution shell (1.92−1.85 Å).

ALR1 residues in the most favored and additional allowed regions, respectively.[41,42] The statistics of stereochemistry and geometry of the final model are shown in Table 1.

Inhibitor-Binding Site. Fidarestat is bound to the active site of ALR1 with its cyclic imide moiety anchored in the anion-binding site, resulting in the clear electron density observed for the inhibitor (Figure 1). The carbonyl oxygen atoms are present within hydrogen-bonding distances from the Nϵ1 atom of Trp114 (2.91 Å) and the OH group of Tyr50 (2.37 Å), while the Nϵ2 atom of His113 forms a hydrogen bond with the 1′-position nitrogen atom in the cyclic imide substituent (2.85 Å). A stereodiagram of fidarestat's binding site is shown in Figure 2. The hydrogen-bonding interactions between the cyclic imide moiety of fidarestat and ALR1 are conserved in the ALR2 structure, which includes an additional hydrogen bond between the main chain N atom of Leu300, a residue lining the "specificity pocket", and the exocyclic amide (carbamoyl) oxygen of fidarestat.[36] In ALR1, Leu300 is a Pro that cannot form a similar hydrogen bond with the exocyclic amide group. A superposition of the ALR1 and ALR2 active sites with the bound fidarestat molecules is shown in Figure 2. While the side chain orientations for the anion-binding
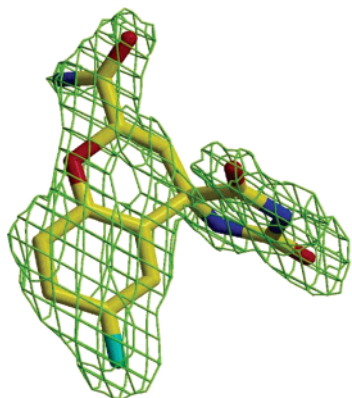
Figure 1. Omit electron density map ($F_o - F_c$) calculated at 1.85 Å resolution with a 2.5σ cutoff superimposed on fidarestat. The figure was prepared using Raster 3D: Photorealistic Molecular Graphics.[60]

site residues Tyr50, His113, and Trp114 are conserved, the electron density indicates a disordered double conformation (Figure 3) for the indole ring of Trp220 in ALR1 that may have resulted from a short contact interaction with the flexible exocyclic amide group, inducing the major conformation (80% occupancy). The two conformations have van der Waals contacts with the exocyclic amide group equal to 2.99 and 3.59 Å, respectively. The former short contact is likely to be contributing to a less favored inhibitor binding compared to ALR2, where a single conformation was observed that has a van der Waals contact with the exocyclic amide group equal to 3.61 Å. The correlation between the electrostatic component of the binding enthalpy (ΔH) and the binding constants measured in solution (IC_{50}) for fidarestat was examined for ALR1 and ALR2. Estimates of the electrostatic interactions between the residues Tyr50, His113, Trp114, and Leu300 (Pro301 in ALR1) and the inhibitor were obtained from molecular modeling. Additionally, for comparison and to illustrate the role of the exocyclic amide group in inhibitor binding to ALR1 and ALR2, the IC_{50} values of the 2R,4S-isomer and sorbinil for the two enzymes are provided in Table 2.

A comparison between the structures of the ALR2 complexes with fidarestat (2S,4S) and its 2R,4S-isomer shows differences in the interaction between the exocyclic amide group and the C-terminal loop residues.[43] While the hydrogen bond between the exocyclic amide group of the compounds and the main chain nitrogen atom of Leu300 is conserved in the fidarestat and the 2R,4S-structures, an induced rotation in the exocyclic amide group occurred to accommodate the 2R,4S into the binding site, resulting in a short contact with Trp219 (2.79 Å versus 3.61 Å with fidarestat). This observation was predicted in an earlier study[44] where the modeling of the 2R,4S-isomer in the active site of ALR2 suggested that both fidarestat and the 2R,4S-isomer bind to ALR2 in a similar manner and that the stereochemistry of the exocyclic amide group may influence the affinity of the compounds for the enzyme. Moreover, a comparison of the IC_{50} values of fidarestat, the 2R,4S-isomer, and sorbinil for the rat ALR2 (Table 2) confirms that the exocyclic amide group in the S-configuration (IC_{50} = 0.035 μM) is optimally positioned to form a hydrogen bond and van der Waals contacts with Leu300 and

Trp219, respectively. The missing exocyclic amide group in sorbinil (IC_{50} = 0.90 μM) and the short contact between the exocyclic amide group of the isomer in the R-configuration (IC_{50} = 0.57 μM) and the side chain of Trp219 were suggested to account for the weaker binding of both sorbinil and the 2R,4S-isomer to ALR2.

Inhibitor Selectivity between ALR1 and ALR2. The inhibitory activities of sorbinil against porcine and human ALR1 are similar to those reported for human and rat ALR2 (Table 2), which have a conserved inhibitor-binding site. This is not surprising when considering that sorbinil lacks the exocyclic amide group that is responsible for the difference in fidarestat's potency for the two enzymes and that the hydrogen-bonding interactions between the cyclic imide moiety of the inhibitor and the active site residues Tyr50, His113, and Trp114 are conserved. Significant selectivity for ALR2 over ALR1 is observed with respect to the more potent ALR2 inhibitors, the 2R,4S-isomer, and particularly fidarestat (2S,4S). The crystal structures of the two enzymes in complex with fidarestat suggest that the 278-fold difference in the binding of inhibitor to porcine ALR1 and human ALR2 is due to both the additional hydrogen bond present between the main chain nitrogen atom of Leu300 and the more favored van der Waals contact between the exocyclic amide group and the side chain of Trp220 in ALR2. In the case of 2R,4S binding, the inability of Pro301 to form a hydrogen bond with the exocyclic amide group of the compound in porcine ALR1 is the likely factor that accounts for the 31-fold difference in potency with the rat ALR2. Additionally, similar to ALR2, the R-configuration of the exocyclic amide group may result in a less favored interaction with the side chain of Trp220 in ALR1, as suggested by the IC_{50} values. An estimation of the electrostatic interactions between fidarestat and Tyr50, His113, Trp114, and Leu300 (Pro301 in ALR1) was obtained from molecular modeling (Table 2). The values for the binding enthalpies (ΔH) for porcine ALR1 and human ALR2 were equal to -12 and -15 kcal/mol with corresponding IC_{50} values of 2.5 and 0.009 μM, respectively. These values, together with the crystal structures, suggest that while the hydrogen-bonding interaction between the main chain nitrogen atom of Leu300 and the exocyclic amide group of fidarestat in ALR2 plays an important role in inhibitor binding and selectivity, it does not account for the full difference in the binding for the two enzymes. The only other observed significant difference in the ALR1 and ALR2 structures is the interaction between the exocyclic amide group and the side chain of Trp220, which is ordered in ALR2 but adopts a disordered double conformation in ALR1, with the minor conformation (20% occupancy) similar to that of Trp219 in ALR2. Therefore, it is likely that this interaction contributes to a less favored inhibitor binding to ALR1.

The binding of fidarestat to ALR1 and ALR2 does not induce a conformational change in the C-terminal loop region of the enzymes, unlike the binding of tolrestat, a carboxylic acid inhibitor that is 180-fold more potent against ALR2 than ALR1, and its structure in complex with both enzymes is known.[32,38] The difference in inhibitor potency was investigated by molecular modeling and mass spectrometry[34] and was attributed to the
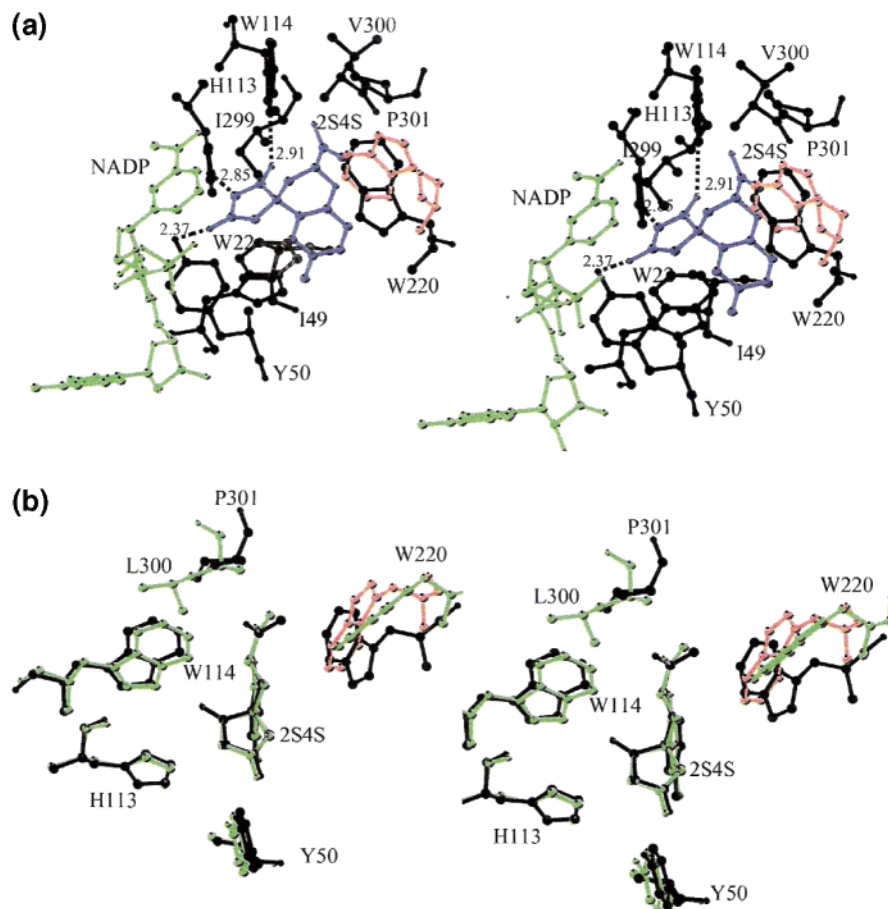
Figure 2. Stereodiagrams showing the binding site of fidarestat (2*S*,4*S*). (a) ALR1 residues within 4 Å and hydrogen bonds as dashed lines with distances given in anstroms are shown. The two conformations for Trp 220 are included. (b) Superposition of the inhibitor binding-site residues Tyr50, His113, Trp114, Trp220, and Pro301 (Leu300 in ALR2) in ALR1 (black and red) and ALR2 (green). Figures were prepared using Molscript.[61]
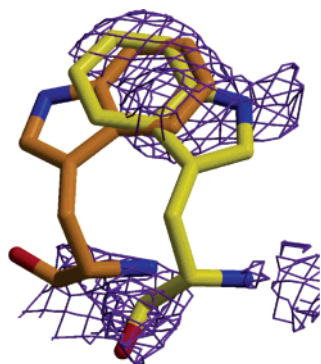
Figure 3. Electron density map $(2F_o - F_c)$ calculated at 1.85 Å resolution with a 1.0σ cutoff superimposed on Trp220. Both conformations for the side chain indole ring are shown. The brown Trp220 (20% occupancy) in this figure is the one shown in red in Figure 2 and has an orientation similar to that of Trp219 of ALR2. The yellow Trp220 is the major conformation (80% occupancy) and is shown in black in Figure 2. The figure was prepared using Raster 3D: Photorealistic Molecular Graphics.[60]

Table 2. Comparisons of ALR1 and ALR2 Inhibitor Binding Constants IC_{50} and ΔH

| | IC_{50} (μM) | | | | ΔH (kcal/mol) | |
inhibitor	porcine ALR1	human ALR1	human ALR2	rat ALR2	porcine ALR1	human ALR2
fidarestat	2.5	1.2[a]	0.009[a]	0.035[c]	−12	−15
sorbinil	4.0	5.4[b]	2.0[b]	0.90[c]		
2*R*,4*S*-isomer	17.8			0.57[c]		

[a] IC_{50} values reported by Mizuno et al.[57] [b] IC_{50} values reported by Barski et al.[58] [c] IC_{50} values reported by Yamaguchi et al.[59]

difference in the hydrophobic interactions between the inhibitor and C-terminal loop region of ALR1 and ALR2. Upon binding of tolrestat to ALR1, the side chain of the nonconserved Arg312, a residue that shares a hydrogen-bonded water molecule with fidarestat's chroman ring, moves to accommodate tolrestat into the binding site. In the ALR2-tolrestat structure, the side chains of

Leu300 and Phe122 move apart from each other, allowing for the binding to occur. A more recent study showed that the cyclic imide inhibitor minalrestat binds to ALR2 with its isoquinoline ring system located in a hydrophobic pocket formed mainly by the side chains of Trp20, Phe122, and Trp219 (Scheme 2).[36] The 4-bromo-2-fluorobenzyl group enters the crevice formed between Phe122, Leu300, and Trp111. The benzyl group π-stacks against the side chain of Trp111, while the bromine atom is positioned within an interacting distance with the side chain of Thr113 and the fluorine interacts with the main chain amide of Leu300. A comparison of the crystal structures of ALR2 in complex with minalrestat and the carboxylic acid inhibitor statil (Scheme 2) showed that these two inhibitors bind to the enzyme in a similar manner, resulting in a conformational change in the side chains of Leu300 and Phe122, suggesting that the orientations of the cyclic imide and carboxylic

Scheme 2

Statil   Minalrestat
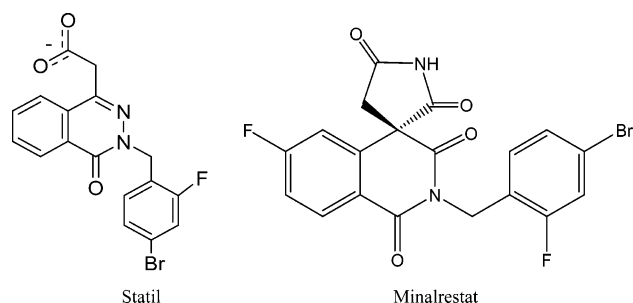
acid inhibitors in the active site of ALR2 are dictated by both the hydrophobic ring system and the polar headgroups of the inhibitors.[35,36]

Our recent molecular modeling and design studies suggest that the replacement of both the fluorine atom of minalrestat and the exocyclic amide group of fidarestat with a carboxylate functional group may enhance the net binding energies of the enzyme–inhibitor complexes by capturing the maximal interactions with nonconserved residues from the C-terminal loop of ALR2.[45] Of particular interest is the unsuccessful attempt to model the minalrestat-based compound into the active site of ALR1 due to steric hindrance between the compound and nonconserved residues from the C-terminal loop, and therefore, this compound may show more selectivity toward ALR2 over ALR1. The result of the present study is in agreement with our earlier assumption[34,45] that while the interactions between the polar head of the inhibitors and the active-site residues play a major role in the overall stability of the enzyme–inhibitor complexes, the compounds that capture the maximal interactions with the nonconserved residues of the ALR2 C-terminal loop region (such as Leu300) provide the basis for the development of more specific inhibitors for ALR2.

Summary

The structure of ALR1 in complex with the potent ARI fidarestat was determined at high resolution to explain the difference in the inhibitor potency between ALR1 and ALR2, an enzyme implicated in the development of the complications of diabetes, and its structure in complex with fidarestat has recently been solved at ultrahigh resolution.[36] In both enzymes, fidarestat is anchored through its cyclic imide ring to the active site and the hydrogen-bonding network with the active-site residues Tyr50, His113, and Trp114 is conserved. The exocyclic amide group of fidarestat forms a hydrogen bond with the main chain N atom of Leu300 in ALR2. This residue is a Pro in ALR1 that cannot form a similar hydrogen bond, allowing for the free rotation of the exocyclic amide group. The interaction between Trp220 of ALR1 and the exocyclic amide group results in a disordered split conformation for the side chain of Trp220, making inhibitor binding less favorable compared to ALR2. The analysis of the binding enthalpy (ΔH) and the in-solution binding constants (IC_{50}) for fidarestat, its 2R,4S-isomer, and sorbinil for ALR1 and ALR2 suggests that the 278-fold difference between fidarestat's potency for the enzymes is the result of both the electrostatic interaction of the exocyclic amide group with Leu300 and the favored van der Waals contact with

Trp219 in ALR2. This is in agreement with the recent results obtained from the structure of the complex between fidarestat and the Leu300Pro mutant form of ALR2[46] where the only observed difference with the wild-type structure[36] is the loss of the H-bond with Leu300, resulting in a 23-fold difference in inhibitor potency.

Experimental Section

Purification of Porcine ALR1. ALR1 was purified by using a modification of a published procedure.[34] Porcine kidneys were diced and homogenized in sodium phosphate (pH 7) buffer containing 5 mM 2-mercaptoethanol and 5 mM EDTA (buffer A). This and all subsequent steps, excluding the FPLC step, were carried out at 4 °C. The homogenate was centrifuged, and the supernatant was treated with ammonium sulfate to obtain both 35% and 65% saturation. The pellet at 65% saturation was resuspended in buffer A and further purified by successive liquid chromatography (LC) steps using affinity Blue Sepharose LC, anionic exchange Q-sepharose LC, gel filtration Superdex 75 FPLC (Pharmacia), and a second Blue Sepharose LC step. The purified enzyme, which was characterized by SDS–polyacrylamide gel electrophoresis (SDS–PAGE) and liquid chromatography–electrospray ionization mass spectrometry (LC–ESMS), was then desalted by repeated dilution–concentration cycles in a Megafuge 1.0R centrifuge (Heraeus) at 3200g with 5 mM Tris (pH 6.5) buffer containing 5 mM 2-mercaptoethanol (buffer B) in a 10 kDa Amicon ultra-4 centrifugal filter unit (Millipore). The sample was finally concentrated to a protein concentration of between 15 and 17 mg/mL.

Crystallization. Crystals of the holoenzyme were grown at 295 K by vapor diffusion using the hanging drop method.[47] Protein in buffer B was first mixed with NADPH to give a 1:20 ratio of protein to cofactor. Each droplet consisted of 5 μL of the protein/NADPH mixture and mixed with 5 μL of solution from the well (2.0 M ammonium sulfate and 0.1 M Tris HCl buffer, pH 8.1; buffer C). Crystals grew to their maximum dimensions (0.30 mm × 0.10 mm × 0.10 mm) within 1 week. Binary crystals were then soaked in a 5 μL droplet of buffer C containing the cyclic imide inhibitor fidarestat, dissolved in dimethyl sulfoxide (DMSO) at a concentration of 2 mM and a final DMSO concentration of 2%, for a period of 10 days. The ternary complex crystals were mounted onto a nylon loop (Hampton) and then briefly immersed into a cryoprotecting solution (20% glycerol in 2.2 M ammonium sulfate and 0.1 M Tris HCl buffer, pH 8.1) before being flash-frozen in liquid nitrogen for X-ray diffraction studies.

In Vitro Inhibitor Evaluation. The IC_{50} value, which is the inhibitor concentration that reduces enzyme activity by 50%, was determined for ALR1 with respect to fidarestat (2S,4S), the 2R,4S-isomer, and sorbinil. Enzyme activity was measured at 25 °C and by monitoring the decrease in NADPH absorbance at 340 nm using DL-glyceraldehyde as substrate in the presence or absence of the compound of interest. The substrate concentration giving the maximum activity was held constant, while that of the inhibitor was varied. The IC_{50} values were estimated from nonlinear regression analyses of percent inhibition versus inhibitor concentration graphs.

X-ray Data Collection and Processing. The holoenzyme crystallized in the hexagonal $P6_522$ space group, with unit cell parameters $a = b = 67.35$ Å, $c = 244.74$ Å, $\alpha = \beta = 90.0°$, and $\gamma = 120.0°$ (at 100 K). There was one monomer per asymmetric unit, consisting of 324 amino acid residues. The solvent content was estimated to occupy 45% of the unit cell volume.[48] A near-completion synchrotron data set was collected at the Swiss Light Source beamline X06SA from one ALR1 ternary complex crystal and processed using the programs HKL2000 and SCALEPACK.[49] The exposure time (3 s), oscillation range (0.3°), and crystal–detector distance (120 mm) were adjusted to optimize the data set. The crystal proved to be resistant to radiation damage at 100 K, allowing the measurement of a 65° zone in reciprocal space for a near-complete data set at a

resolution of 1.85 Å. Data collection and processing statistics are shown in Table 1.

Structure Refinement. The coordinates of the porcine ALR1 holoenzyme structure[50] were used to solve the structure by molecular replacement.[51] Crystallographic refinement involved repeated cycles of conjugate gradient energy minimization, simulated annealing, and temperature factor refinement.[51] Amino acid side chains were fitted into $2F_o - F_c$ and $F_o - F_c$ electron density maps. The final $F_o - F_c$ maps (Figure 1) indicated clear electron density for fidarestat. Water molecules were fitted into a difference map, and final cycles of the conjugate gradient refinement were carried out using the SHELX program package.[52] The programs TURBO-FRODO[53] and XtalView/Xfit[54] were used for fitting the models into the electron density. The difference electron density maps allowed the identification of multiple conformations for several amino acid residue side chains including Trp220 (Figure 3). Refinement statistics are presented in Table 1.

Molecular Modeling Calculations. Energy minimization was carried out on the structures of the ternary complexes of ALR1 and ALR2 using the Discover 2.7 package (Biosym Technologies, San Diego, CA) on an O2 (R12000) workstation (Silicon Graphics, Mountain View, CA) following established procedures found to be effective in examining conformational space with a protein–ligand complex.[55,56] Arginine, lysine, aspartate, and glutamate amino acids were charged, while the histidines were uncharged. Consistent with the mechanism proposed for the binding of fidarestat to ALR2,[36] where the inhibitor is initially bound in a neutral state, His113 was singly protonated at the Nδ1 atom and the inhibitor was uncharged. The constant valence force field incorporating the simple harmonic function for bond stretching and excluding all nondiagonal terms was used (cutoff distance of 31 Å). Calculations were done using the algorithms' steepest descents and conjugate gradients (down to a maximum atomic root-mean-square derivative of 10.0 and 0.01 kcal/Å, respectively). The structures were visualized by using InsightII, and the contributions of the inhibitor-binding site residues Tyr50, His113, Trp114, and Pro301 (Leu300 in ALR2) to the binding in the ALR1 and ALR2 ternary complexes were calculated by using Discover (Table 2).

The atomic coordinates will be deposited in the Protein Data Bank and will be released immediately upon publication.

References

(1) Srivastava, S.; Spite, M.; Trent, J. O.; West, M. B.; Ahmed, Y.; Bhatnagar, A. Aldose reductase-catalyzed reduction of aldehyde phospholipids. *J. Biol. Chem.* **2004**, *279*, 53395–53406.

(2) Hayashi, H.; Fujii, Y.; Watanabe, K.; Urade, Y.; Hayaishi, O. Enzymatic conversion of prostaglandin H2 to prostaglandin F2 alpha by aldehyde reductase from human liver: comparison to the prostaglandin F synthetase from bovine lung. *J. Biol. Chem.* **1989**, *264*, 1036–1040.

(3) Matsuura, K.; Shiraishi, H.; Hara, A.; Sato, K.; Deyashiki, Y.; Ninomiya, M.; Sakai, S. Identification of a principal mRNA species for human 3alpha-hydroxysteroid dehydrogenase isoform (AKR1C3) that exhibits high prostaglandin D2 11-ketoreductase activity. *J. Biochem. (Tokyo)* **1998**, *124*, 940–946.

(4) Hung, C. F.; Penning, T. M. Members of the nuclear factor 1 transcription factor family regulate rat 3alpha-hydroxysteroid/dihydrodiol dehydrogenase (3alpha-HSD/DD AKR1C9) gene expression: a member of the aldo-keto reductase superfamily. *Mol. Endocrinol.* **1999**, *13*, 1704–1717.

(5) Nelson, V. L.; Qin Kn, K. N.; Rosenfield, R. L.; Wood, J. R.; Penning, T. M.; Legro, R. S.; Strauss, J. F., III; McAllister, J. M. The biochemical basis for increased testosterone production in theca cells propagated from patients with polycystic ovary syndrome. *J. Clin. Endocrinol. Metab.* **2001**, *86*, 5925–5933.

(6) Gavidia, I.; Perez-Bermudez, P.; Seitz, H. U. Cloning and expression of two novel aldo-keto reductases from Digitalis purpurea leaves. *Eur. J. Biochem.* **2002**, *269*, 2842–2850.

(7) Steckelbroeck, S.; Jin, Y.; Oyesanmi, B.; Kloosterboer, H. J.; Penning, T. M. Tibolone is metabolized by the 3alpha/3beta-hydroxysteroid dehydrogenase activities of the four human isozymes of the aldo-keto reductase 1C subfamily: inversion of stereospecificity with a delta5(10)-3-ketosteroid. *Mol. Pharmacol.* **2004**, *66*, 1702–1711.

(8) Ji, Q.; Aoyama, C.; Nien, Y. D.; Liu, P. I.; Chen, P. K.; Chang, L.; Stanczyk, F. Z.; Stolz, A. Selective loss of AKR1C1 and AKR1C2 in breast cancer and their potential effect on progesterone signaling. *Cancer Res.* **2004**, *64*, 7610–7617.

(9) Hara, A.; Deyashiki, Y.; Nakayama, T.; Sawada, H. Isolation and characterization of multiforms of aldehyde reductase in chicken kidney. *Eur. J. Biochem.* **1983**, *133*, 207–214.

(10) Sawada, H.; Hara, A.; Nakayama, T.; Kato, F. Reductases for aromatic aldehydes and ketones from rabbit liver. Purification and characterization. *J. Biochem. (Tokyo)* **1980**, *87*, 1153–1165.

(11) Wermuth, B.; Munch, J. D.; von Wartburg, J. P. Purification and properties of NADPH-dependent aldehyde reductase from human liver. *J. Biol. Chem.* **1977**, *252*, 3821–3828.

(12) Sawada, H.; Hara, A.; Nakayama, T.; Hayashibara, M. Kinetic mechanisms in the reduction of aldehydes and ketones catalyzed by rabbit liver aldehyde reductases and hydroxysteroid dehydrogenases. *J. Biochem. (Tokyo)* **1982**, *92*, 185–191.

(13) Jez, J. M.; Flynn, T. G.; Penning, T. M. A new nomenclature for the aldo-keto reductase superfamily. *Biochem. Pharmacol.* **1997**, *54*, 639–647.

(14) Warren, J. C.; Murdock, G. L.; Ma, Y.; Goodman, S. R.; Zimmer, W. E. Molecular cloning of testicular 20 alpha-hydroxysteroid dehydrogenase: identity with aldose reductase. *Biochemistry* **1993**, *32*, 1401–1406.

(15) Dixit, B. L.; Balendiran, G. K.; Watowich, S. J.; Srivastava, S.; Ramana, K. V.; Chang, L.; Stanczyk, F. Z.; Stolz, A. Kinetic and structural characterization of the glutathione-binding site of aldose reductase. *J. Biol. Chem.* **2000**, *275*, 21587–21595.

(16) Tabakoff, B.; Erwin, V. G. Purification and characterization of a reduced nicotinamide adenine dinucleotide phosphate-linked aldehyde reductase from brain. *J. Biol. Chem.* **1970**, *245*, 3263–3268.

(17) Tulsiani, D. R.; Touster, O. Resolution and partial characterization of two aldehyde reductases of mammalian liver. *J. Biol. Chem.* **1977**, *252*, 2545–2550.

(18) Flynn, T. G.; Shires, J.; Walton, D. J. Properties of the nicotinamide adenine dinucleotide phosphate-dependent aldehyde reductase from pig kidney. Amino acid composition, reactivity of cysteinyl residues, and stereochemistry of D-glyceraldehyde reduction. *J. Biol. Chem.* **1975**, *250*, 2933–2940.

(19) El-Kabbani, O.; Wilson, D. K.; Petrash, M.; Quiocho, F. A. Structural features of the aldose reductase and aldehyde reductase inhibitor-binding sites. *Mol. Vision* **1998**, *4*, 19–25.

(20) Bohren, K. M.; Grimshaw, C. E.; Gabbay, K. H. Catalytic effectiveness of human aldose reductase. Critical role of C-terminal domain. *J. Biol. Chem.* **1992**, *267*, 20965–20970.

(21) Barski, O. A.; Gabbay, K. H.; Bohren, K. M. The C-terminal loop of aldehyde reductase determines the substrate and inhibitor specificity. *Biochemistry* **1996**, *35*, 14276–14280.

(22) Sato, S.; Kador, P. F. Inhibition of aldehyde reductase by aldose reductase inhibitors. *Biochem. Pharmacol.* **1990**, *40*, 1033–1042.

(23) Narayanan, S. Aldose reductase and its inhibition in the control of diabetic complications. *Ann. Clin. Lab. Sci.* **1993**, *23*, 148–158.

(24) Williamson, J. R.; Chang, K.; Frangos, M.; Hasan, K. S.; Ido, Y.; Kawamura, T.; Nyengaard, J. R.; van den Enden, M.; Kilo, C.; Tilton, R. Hyperglycemic pseudohypoxia and diabetic complications. *Diabetes* **1993**, *42*, 801–813.

(25) Gonzalez, A. M.; Sochor, M.; Hothersall, J. S.; McLean, P. Effect of aldose reductase inhibitor (sorbinil) on integration of polyol pathway, pentose phosphate pathway, and glycolytic route in diabetic rat lens. *Diabetes* **1986**, *35*, 1200–1205.

(26) Lee, A. Y.; Chung, S. K.; Chung, S. S. Demonstration that polyol accumulation is responsible for diabetic cataract by the use of transgenic mice expressing the aldose reductase gene in the lens. *Proc. Natl. Acad. Sci. U.S.A.* **1995**, *92*, 2780–2784.

(27) Oates, P. J. Polyol pathway and diabetic peripheral neuropathy. *Int. Rev. Neurobiol.* **2002**, *50*, 325–392.

(28) Sato, S. Rat kidney aldose reductase and aldehyde reductase and polyol production in rat kidney. *Am. J. Physiol.* **1992**, *263*, F799–F805.

(29) Foppiano, M.; Lombardo, G. Worldwide pharmacovigilance systems and tolrestat withdrawal. *Lancet* **1997**, *349*, 399–400.

(30) Feather, M. S.; Flynn, T. G.; Munro, K. A.; Kubiseski, T. J.; Walton, D. J. Catalysis of reduction of carbohydrate 2-oxoaldehydes (osones) by mammalian aldose reductase and aldehyde reductase. *Biochim. Biophys. Acta* **1995**, *1244*, 10−16.

(31) Ratliff, D. M.; Van der Jagt, D. J.; Eaton, R. P.; Van der Jagt, D. L. Increased levels of methylglyoxal-metabolizing enzymes in mononuclear and polymorphonuclear cells from insulin-dependent diabetic patients with diabetic complications: aldose reductase, glyoxalase I, and glyoxalase II-a clinical research center study. *J. Clin. Endocrinol. Metab.* **1996**, *81*, 488−492.

(32) El-Kabbani, O.; Carper, D. A.; McGowan, M. H.; Devedjiev, Y.; Rees-Milton, K. J.; Flynn, T. G. Studies on the inhibitor-binding site of porcine aldehyde reductase: crystal structure of the holoenzyme-inhibitor ternary complex. *Proteins* **1997**, *29*, 186−192.

(33) El-Kabbani, O.; Old, S. E.; Ginell, S. L.; Carper, D. A. Aldose and aldehyde reductases: structure−function studies on the coenzyme and inhibitor-binding sites. *Mol. Vision* **1999**, *5*, 20−26.

(34) El-Kabbani, O.; Rogniaux, H.; Barth, P.; Chung, R. P. T.; Fletcher, E. V.; Van Dorsselaer, A.; Podjarny, A. Aldose and aldehyde reductases: correlation of molecular modelling and mass spectrometric studies on the binding of inhibitors to the active site. *Proteins* **2000**, *41*, 407−414.

(35) El-Kabbani, O.; Ramsland, P.; Darmanin, C.; Chung, R.; Podjarny, A. Structure of human aldose reductase holoenzyme in complex with statil: an approach to structure-based inhibitor design of the enzyme. *Proteins* **2003**, *50*, 230−238.

(36) El-Kabbani, O.; Darmanin, C.; Schneider, T. R.; Hazemann, I.; Ruiz, F.; Oka, M.; Joachimiak, A.; Schulze-Briese, C.; Tomizaki, T.; Mitschler, A.; Podjarny, A. Ultra-high resolution drug design II: atomic resolution structures of human aldose reductase holoenzyme complexed with fidarestat and minalrestat; implications for the binding of cyclic imide inhibitors. *Proteins* **2004**, *55*, 805−813.

(37) Wilson, D. K.; Tarle, I.; Petrash, J. M.; Quiocho, F. A. Refined 1.8 Å structure of human aldose reductase complexed with the potent inhibitor zopolrestat. *Proc. Natl. Acad. Sci. U.S.A.* **1993**, *90*, 9847−9851.

(38) Urzhumtsev, A.; Tête-Favier, F.; Mitschler, A.; Barbanton, J.; Barth, P.; Urzhumtseva, J. F.; Biellmann, A. D.; Podjarny, A.; Moras, D. A. "Specificity" pocket inferred from the crystal structures of the complexes of aldose reductase with the pharmaceutically important inhibitors tolrestat and sorbinil. *Structure* **1997**, *5*, 601−612.

(39) El-Kabbani, O.; Green, N. C.; Lin, G.; Carson, M.; Narayana, S. V.; Moore, K. M.; Flynn, T. G.; DeLucas, L. J. Structures of human and porcine aldehyde reductase: an enzyme implicated in diabetic complications. *Acta Crystallogr, Sect. D: Biol. Crystallogr.* **1994**, *50*, 859−868.

(40) Ye, Q.; Hyndman, D.; Green, N.; Li, X.; Korithoski, B.; Jia, Z.; Flynn, T. G. Crystal structure of an aldehyde reductase Y50F mutant-NADP complex and its implications for substrate binding. *Proteins* **2001**, *44*, 12−19.

(41) Laskowski, R. A.; MacArthur, M. W.; Moss, D. S.; Thornton, J. M. PROCHECK: a program to check the stereochemical quality of protein structures. *J. Appl. Crystallogr.* **1993**, *26*, 283−291.

(42) Ramachandran, G. N.; Sasisekharan, V. Conformation of proteins and polypeptides. *Adv. Protein Chem.* **1968**, *23*, 283−437.

(43) El-Kabbani, O.; Darmanin, C.; Oka, M.; Schulze-Briese, C.; Tomizaki, T.; Hazemann, I.; Mitschler, A.; Podjarny, A. High-resolution structures of human aldose reductase holoenzyme in complex with stereoisomers of the potent inhibitor fidarestat: stereospecific interaction between the enzyme and a cyclic imide type inhibitor. *J. Med. Chem.* **2004**, *47*, 4530−4537.

(44) Oka, M.; Matsumoto, Y.; Sugiyama, S.; Tsuruta, N.; Matsushima, M. A potent aldose reductase inhibitor, (2*S*,4*S*)-6-fluoro-2′,5′-dioxyspiro[chroman-4,4′-imidazoline]-2-carboxamide (fidar-

estat): its absolute configuration and interaction with aldose reductase by X-ray crystallography. *J. Med. Chem.* **2000**, *43*, 2479−2483.

(45) Darmanin, C.; Chevreux, G.; Potier, N.; Van Dorsselaer, A.; Hazemann, I.; Podjarny, A.; El-Kabbani, O. Probing the ultra-high resolution structure of aldose reductase with molecular modelling and noncovalent mass spectrometry. *Bioorg. Med. Chem.* **2004**, *12*, 3797−3806.

(46) Petrova, T.; Steuber, H.; Hazemann, I.; Cousido, A.; Mitschler, A.; Chung, R.; Oka, M.; Klebe, G.; El-Kabbani, O.; Joachimiak, A.; Podjarny, A. Factorizing selectivity determinants of inhibitor binding towards aldose and aldehyde reductases: structural and thermodynamic properties of the ALR2 mutant Leu300Pro/fidarestat complex. *J. Med. Chem.*, accepted.

(47) McPherson, A. Crystallization of macromolecules: general principles. *Methods Enzymol.* **1985**, *114*, 112−120.

(48) Matthews, B. W. Solvent content of protein crystals. *J. Mol. Biol.* **1968**, *33*, 491−497.

(49) Otwinowski, Z.; Minor, W. Processing of X-ray diffraction data collected in oscillation mode. *Methods Enzymol.* **1997**, *276*, 307−326.

(50) El-Kabbani, O.; Judge, K.; Ginell, S. L.; Myles, D. A.; DeLucas, L. J.; Flynn, T. G. Structure of porcine aldehyde reductase holoenzyme. *Nat. Struct. Biol.* **1995**, *2*, 687−692.

(51) Brünger, A. T.; Krukowski, A.; Erickson, J. W. Slow-cooling protocols for crystallographic refinement by simulated annealing. *Acta Crystallogr. A* **1990**, *46*, 585−593.

(52) Sheldrick, G.; Schneider, T. SHELXL: high-resolution refinement. *Methods Enzymol.* **1997**, *277*, 319−343.

(53) Roussel, A.; Cambillau, C. TURBO-FRODO Molecular Graphics Program. In *Silicon Graphics Geometry Partner Directory*; Silicon Graphics: Mountain View, CA, 1989; pp 77−78.

(54) McRee, D. E. XtalView/Xfit. A versatile program for manipulating atomic coordinates and electron density. *J. Struct. Biol.* **1999**, *125*, 156−165.

(55) Darmanin, C.; El-Kabbani, O. Modelling studies of the active site of human sorbitol dehydrogenase: an approach to structure-based inhibitor design of the enzyme. *Bioorg. Med. Chem. Lett.* **2001**, *11*, 3133−3136.

(56) Darmanin, C.; El-Kabbani, O. Modelling studies on the binding of substrate and inhibitor to the active site of human sorbitol dehydrogenase. *Bioorg. Med. Chem. Lett.* **2000**, *10*, 1101−1104.

(57) Mizuno, K.; Yamaguchi, T.; Unoue, A.; Tomiya, N.; Unno, R.; Miura, K.; Usui, T.; Matsumoto, Y.; Kondo, Y.; Yoshina, S.; Kondo, Y.; Sato, M.; Matsubara, A.; Kato, N.; Nakano, K.; Shirai, M.; Inoue, T.; Awaya, J.; Asaeda, N.; Hayasaka, I.; Koide, M.; Hibi, C.; Ban, M.; Sawai, K.; Kurono, M. Profile of a new aldose reductase inhibitor (2*S*,4*S*)-6-fluoro-2′,5′-dioxyspiro[chroman-4,4′-imidazoline]-2-carboxamide. *Excerpta Med.* **1990**, *913*, 89−96.

(58) Barski, O. A.; Gabbay, K. H.; Grimshaw, C. E.; Bohren, K. M. Mechanism of human aldose reductase: characterization of the active site pocket. *Biochemistry* **1995**, *34*, 11264−11275.

(59) Yamaguchi, T.; Miura, K.; Usui, T.; Unno, R.; Matsumoto, Y.; Fukushima, M.; Mizuno, K.; Kondo, Y.; Baba, Y.; Kurono, M. Synthesis and aldose reductase inhibitory activity of 2-substituted-6-fluoro-2,3-dihydrospiro[4H-1-benzopyran-4,4′-imidazolidine]-2′,5′-diones. *Arzneim.-Forsch.* **1994**, *44*, 344−348.

(60) Merritt, E. A.; Bacon, D. J. Raster 3D: photorealistic molecular graphics. *Methods Enzymol.* **1997**, *277*, 505−524.

(61) Kraulis, P. J. MOLSCRIPT: A program to produce both detailed and schematic plots of protein structures. *J. Appl. Crystallogr.* **1991**, *24*, 946−950.